Ecotoxicology and Public Health

Computational Biotransformation Profile of Emerging Phenolic Pollutants by Cytochromes P450: Phenol Coupling Mechanism

Fangjie Guo, Lihong Chai, Shubin Zhang, Haiying Yu, Weiping Liu, Kasper P. Kepp, and Li Ji

Environ. Sci. Technol., **Just Accepted Manuscript** • DOI: 10.1021/acs.est.9b06897 • Publication Date (Web): 22 Jan 2020

Computational Biotransformation Profile of Emerging Phenolic Pollutants by Cytochromes P450: Phenol Coupling Mechanism

Fangjie Guo, [1‡] *Lihong Chai,* [1‡] *Shubin Zhang,* [2,3] *Haiying Yu,* [4] *Weiping Liu,* [1] *Kasper P. Kepp,* [5] *and Li Ji** [1,3]

[1] College of Environmental and Resource Sciences, Zhejiang University, Yuhangtang Road 866, Hangzhou 310058, China

[2] CAS Key Laboratory of Tropical Forest Ecology, Xishuangbanna Tropical Botanical Garden, Chinese Academy of Sciences, Mengla, Yunnan 666303, China

[3] Graduate School of Agriculture, Kyoto University, Kitashirakawa Oiwake-cho, Sakyo-ku, Kyoto 606-8502, Japan

[4] College of Geography and Environmental Sciences, Zhejiang Normal University, Yingbin Avenue 688, Jinhua 321004, P.R. China

[5] DTU Chemistry, Technical University of Denmark, Building 206, Kgs. Lyngby, DK-2800, Denmark

Abstract

Phenols are ubiquitous environmental pollutants, whose biotransformation involving phenol coupling catalyzed by cytochromes P450, may produce more lipophilic and toxic metabolites. DFT computations were performed to explore the debated phenol coupling mechanisms, taking triclosan as a model substrate. We find that a diradical pathway facilitated by Compound I and protonated Compound II of P450 is favored vs. alternative radical-addition or electron-transfer mechanisms. The identified diradical coupling resembles a "two-state reactivity" from Compound I characterized by significantly high rebound barriers of the phenoxy radicals, which can be formulated into three equations for calculating the ratio [coupling]/[hydroxylation]. A higher rebound barrier than H-abstraction for triclosan in the high-spin state can facilitate the phenoxy radical dissociation and thus to enable phenol coupling, while H-abstraction/radical-rebound causing phenol hydroxylation via minor rebound barriers mostly occur in the low-spin state. Therefore, oxidation of triclosan by P450 fits the first equation with a ratio [coupling]/[hydroxylation] of 1:4, consistent with experimental data indicating different extents of triclosan coupling (6-40%). The high rebound barrier of phenoxy radicals, as a key for the mechanistic identification of phenol coupling vs. hydroxylation, originates from their weak electron donor ability due to spin aromatic delocalization. We envision that the revealed mechanism can be extended to the cross-coupling reactions between different phenolic pollutants, and the coupling reactions of several other aromatic pollutants, to infer unknown metabolites.

Introduction

Oxidative phenol couplings catalyzed by cytochromes P450 (P450) occur widely during natural product biosynthesis, e.g. phenol couplings are necessary for alkaloid and antibiotic biosynthesis in plants.[1-4] In the meantime, phenolic xenobiotics distribute ubiquitously in the environment,[5-9] such as a significant proportion of pharmaceuticals and personal care products (PPCPs) contain phenolic moieties, and many emerging pollutants with phenolic residues can be formed readily via aromatic hydroxylation, which may undergo P450 biotransformation via phenol coupling to produce more lipophilic metabolites with higher toxicity; for example, more estrogenic products have been detected within and among triclosan and several other phenolic pollutants such as bisphenol A (BPA) in both *in vitro* and *in vivo* assays.[10] A full understanding of these metabolic mechanisms is necessary for accurately estimating the occurrence and possibility of specific phenol coupling reactions, which can then provide the putative metabolites for exploring the potential toxicological effects of phenolic pollutants with susceptibility to metabolism in organisms.

The concept of phenol coupling as a diradical mechanism was proposed as far back as 1957 for alkaloid salutaridine biosynthesis by C-C coupling of *R*-reticuline.[11] With the advancement of P450 chemistry, its active species was recognized as the remarkable iron(IV)-oxo heme cation radical cofactor known as compound I (Cpd I) (**Scheme 1, top**).[12,13] The diradical mechanism, shown in **Scheme 1(i)**, has been thought to involve the initial abstraction of a phenolic H-atom by Cpd I to create a phenoxy radical and the protonated iron-hydroxo species Cpd II. Subsequently, this phenoxy radical rotates or another phenolic substrate approaches in juxtaposition to the iron of protonated Cpd II, leading to abstraction of another phenolic

hydrogen atom and formation of a second phenoxy radical, followed by inter- or intramolecular phenol couplings within a catalytic cycle of the P450 enzyme.[1,14,15]

Scheme 1. Structure of Compound I of P450 and Alternative Mechanisms for Phenol-Coupling Catalyzed by P450

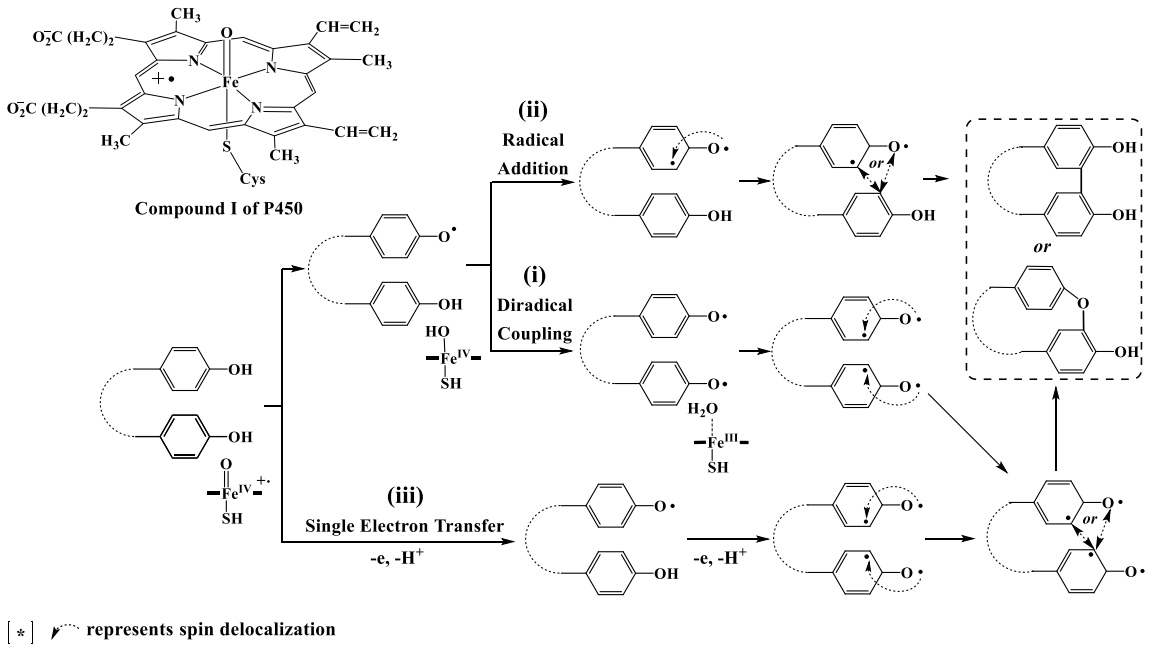

Another possible coupling pathway is radical addition to the π-ring, as shown in **Scheme 1(ii)**.[1] If the diradical or radical addition enables oxidative phenol coupling, the phenoxy radical needs long lifetime. Several studies indicate that the radicals formed in P450-catalyzed oxidative reactions are relatively short-lived and restricted in their motions, in favor of H-abstraction/phenoxy-radical rebound leading to aromatic hydroxylation as supported by the tendency of H-abstraction from phenols.[16-19] Therefore, the major bottleneck to explain the traditionally proposed radical mechanism especially the diradical mechanism is that why normally short-lived radicals herein have enough long lifetime to enable phenoxy radical coupling. In addition, oxidative coupling of phenolic compounds through consecutive electron-transfer (ET) steps is considered the most typical peroxidation reaction catalyzed by peroxidases

77 such as horseradish peroxidase (HRP).[20-23] Since both HRP and P450 are heme enzymes, the
78 possibility that P450 performs oxidative coupling reactions of phenols is of substantial interest,
79 as shown in **Scheme 1(iii)**.[1] We expect that HRP with its computed larger electron affinity of
80 Cpd I (6.41 eV) may more readily participate in ET reactions than P450 (3.06 eV).[24] Therefore,
81 the mechanism of phenol coupling poses a fascinating dilemma.

82 Computational analysis can reveal the electronic structure properties determining
83 transformation mechanisms of environmental pollutants,[25-30] which has been performed on P450
84 oxygenation reactions leading to the concept of two-state reactivity (TSR) of Cpd I to resolve the
85 "rebound controversy" of alkane hydroxylation,[31-36] as well as other mechanistic controversies in
86 alkene epoxidation,[37] nitrosamine denitrosation,[38] alkane desaturation[39] and so on. According to
87 TSR, the alkyl radicals and iron-hydroxy species are produced by Cpd I through H-abstraction
88 on two closely-lying spin surfaces involving a high-spin (HS, quartet) and low-spin (LS, doublet)
89 states, which then react differently; in the LS state, the alkyl radicals rebound onto the iron-
90 hydroxy intermediate to generate the alcohol complex with no product rearrangement since the
91 rebound is essentially barrierless, thus the radical lifetime is negligible whereas in the HS state
92 the barrier for rebound is small but significant (1−5 kcal/mol); accordingly, the radical lifetime is
93 relatively long such that the radical rebound after rearrangement can compete with direct
94 rebound.[31,32,34,40,41] Since the initial H-abstraction is rate-determining in both spin states, the
95 existence of other competitive pathways for alkyl radicals was considered unlikely, although the
96 dissociation of radicals from the P450 active site requires very little energy.[41] However, the
97 radical dissociation pathway has proven prominent in the area of synthetic iron–oxo
98 complexes.[35,42-45] Although phenol coupling by P450 should inherently relate to the non-rebound

99 mechanism, this mechanism, to our knowledge, remains unexplored in the context of P450
100 reactivity.

101 We have recently shown that P450-catalyzed aromatic hydroxylation of bisphenols and
102 alkylphenols proceeds via H-abstraction/phenoxy-radical rebound on the LS surface, due to the
103 fact that the phenoxy radical rebound onto the aromatic ring in the HS state has higher barriers
104 than the initial H-abstraction barrier.[46] Studies of CYP2D6 indicate that dopamine synthesis is
105 facilitated by H-abstraction/phenoxy-radical rebound, with a very high barrier (19 kcal/mol) for
106 the phenoxy radical rebound onto the aromatic ring.[47] However, we hypothesize that these
107 radical-rebound steps can be less favorable than other non-rebound reactions such as phenoxy
108 radical dissociation, which will provide a pathway to generate phenol coupling products. It is
109 unclear whether high rebound barriers of phenoxy radicals are common to P450-catalyzed
110 phenol oxidations and whether this makes phenoxy radical dissociation and phenol coupling
111 products possible. This would greatly affect the mechanistic relationship between phenol
112 coupling and hydroxylation and thus deserves to be addressed in mechanistic detail.

113 In order to elucidate the complete scenario of P450-dependent phenol coupling, we
114 performed density functional theory (DFT) in investigating the phenol coupling reactions.
115 Triclosan, one commonly used antibacterial ingredient and one of the widely concerned PPCP
116 pollutants, was selected to get the complete mechanistic picture of phenol coupling, with
117 available experimental data to confirm the derived mechanisms.[10] As will be shown, this work
118 provides the fundamental insight into how do the phenol coupling reactions catalyzed by P450
119 proceed based on the high rebound barrier of phenoxy radical within the framework of "two-state
120 reactivity", and such coupling mechanism can be mapped to the coupling reactions of several
121 other aromatic pollutants.

122 # Computational Methodology

123 ## Enzymatic Reactions

124 **Level of Theory.** As in previous studies,[39,48,49] the six-coordinate tri-radicaloid ferryl
125 complex $Fe^{4+}O^{2-}(C_{20}N_4H_{12})^{-1}(SH)^{-1}$ was used to model the enzymatic active site of Cpd I of P450.
126 The geometries were optimized with unrestricted DFT using the B3LYP hybrid density
127 functional[50,51] with the LANL2DZ basis set[52] for iron and 6–31G** for other atoms (denoted
128 BSI). B3LYP was used since it can reproduce the measured kinetic isotope effects[53] and electron
129 paramagnetic resonance parameters for penta-coordinated heme,[54] generates geometries
130 consistent with crystal structures,[55] and shows qualitatively accurate relative energies vs.
131 benchmark CASSCF calculations.[56] The basis-set superposition error (BSSE) was shown to be
132 very small for reactant complexes in P450-catalyzed reactions by DFT-B3LYP method,[31] so this
133 work did not consider the minor contributions of BSSE to the energies. The vibrational
134 frequencies were calculated to confirm the nature of all ground states (no imaginary frequencies)
135 and transition states (one imaginary frequency), while the intrinsic reaction coordinate (IRC)
136 approach was used to verify the connection from transition state to its reactant and product. The
137 computed vibrational frequencies were used further for quantifying the zero-point energy
138 correction (ZPE) as well as the thermal contributions to the Gibbs free energy at T = 298.15 K
139 and 1 atm pressure.

140 For better estimating Gibbs free energies, single-point calculations were done using the
141 LANL2DZ basis set for iron and the 6–31+G** basis set augmented with diffuse basis functions
142 for all other atoms (denoted BSII), employing the polarizable continuum solvation model
143 (PCM)[63] using chlorobenzene (ε = 5.7) to include solvation free energies. Chlorobenzene was
144 used because it can provide a good estimate of the polarization caused by the dipoles of the

145 protein pocket near the axial cysteine.[64] Dispersion interactions could be important in the close
146 interaction of the strained phenol rings and were thus considered by single-point calculations
147 with the B3LYP-D3/BSI level since B3LYP itself does not include dispersion.[66] The relative
148 Gibbs free energies of the P450 oxidation reactions shown below were estimated by combining
149 PCM solvation (chlorobenzene) single-point energies at B3LYP/BSII level and dispersion
150 corrections, as well as thermochemical contributions to free energy from optimizations at the BSI
151 level, unless pointed out specifically.

152 **Variation of DFT Functional and Basis Set.** In order to further access the sensitivity of
153 the reaction mechanism toward the choice of density functional, we performed single-point
154 calculations with other hybrid, local, and non-hybrid functionals, i.e. TPSSh,[57,58] B3PW91,[51,59]
155 BLYP,[50,60] MPW1PW91[61] and M06L[62] om the B3LYP/BSI optimized geometries. Whereas
156 absolute barriers and intermediate energies changed to some extent, we found that the relative
157 pathway energies, and thus the reaction preferences and overall qualitative picture were similar
158 with all the functionals (**Table S10**), and the main findings on the relative preference of the
159 pathways are thus insensitive to method choice.

160 To access whether the effect of diffuse basis functions on geometry optimizations influence
161 the mechanism, we reoptimized the inner-sphere oxidation pathway of triclosan in the HS state at
162 the B3LYP/BSII level followed by analytical frequency calculations. The results provide the
163 same mechanistic picture with only minor geometric differences from those done with BSI
164 (**Figure S1**). We also tested the basis set effect of the single-point calculations on the H-
165 abstraction from the phenolic group, O-addition onto the aromatic ring of triclosan, and phenoxy
166 radical rebound steps, using the SDD basis set on iron coupled to the 6–311++G** basis set for

other atoms; the result gives just few energetic discrepancies compared to the results got from the BSII level (**Table S12**).

Variation of Solution and Solvation Model. To evaluate the sensitivity of our results to the solution choice, we calculated PCM energies in cyclohexane (ε = 2.0), 1-bromopropane (ε = 8.0), ethanol (ε = 24.9), and acetonitrile (ε = 35.7), resulting in the same qualitative picture except for a minor energy difference (**Tables S13**). We further tested the bulk polarity effect using the SMD solvation model[65] in chlorobenzene, the results of which shows that the SMD solvation model has very similar solvation effect to that of the PCM solvation model, analyzed from the detailed comparison at both the quantitative and qualitative levels (details see Section II in the Supporting Information, SI).

Protein Environment Effect. The quantum chemical cluster (QCC)[67] and quantum mechanics/molecular mechanics (QM/MM)[68] are two recognized methods in investigating the protein effects of known structure on the catalytic mechanism in enzymatic reactions. However, until now there is no any study reporting the specific P450 isoforms responsible for the intermolecular coupling of phenolic pollutants including triclosan, while human CYP1A2 was shown to have the highest activity in metabolizing triclosan via hydroxylation into 2,4-dichlorophenol, 4-chlorocatechol and 5′-hydroxytriclosan.[69] As mechanism revealed from the small Cpd I model, H-abstraction and high-barrier phenoxy radical rebound are two preconditions for the phenoxy radical dissociation and subsequent phenol coupling. Therefore, the QCC approach was carried out to check the reaction mechanism of H-abstraction and phenoxy radical rebound of triclosan, which treated the active site of CYP1A2 (PDB code: 2HI4) with important surrounding amino acids quantum mechanically (details see Section III in the SI). The QCC approach shows that the cluster model is mechanistically consistent with the Cpd I

model (H-abstraction is much more favorable than O-addition, followed by phenoxy radical rebound with very high rebound barrier), namely, the geometric constraints near the active site of CYP1A2 do not restrict the preferred pathways obtained from the small model.

Non-Enzymatic Reactions

Radical Addition and Diradical Coupling Reactions. All geometries of various reactions were optimized at the B3LYP/BSI level in both the polar (water solution, ε = 78.4) and non-polar (chlorobenzene solution, ε = 5.7) environments with PCM. Single-point energies were computed with PCM for both water and chlorobenzene with D3 dispersion corrections at the B3LYP/6-311++G** level. The reported reaction free energies for reactions were described by B3LYP/BSIII single-point energies with solution and D3 dispersion corrections, as well as free energy corrections from B3LYP/BSI geometry optimizations.

Molecular Property Computations. Ionization potentials (IPs), electron affinities (EAs) and bond dissociation energies (BDEs) were obtained from the molecules optimized at the B3LYP/BSI level in the gas phase, using single-point calculations at the B3LYP/BSIII level with free energy corrections for IPs and EAs, and enthalpy corrections for the BDEs.

All computations of this work were performed using the Gaussian 09 D.01 program.[70]

Results and Discussion

Outer-Sphere Oxidation Mechanism

We firstly focused on the mechanism of outer-sphere ET from the electron-rich phenolic group of triclosan to Cpd I of P450 producing the phenolic radical-cation and Cpd II, according to eq. (1):

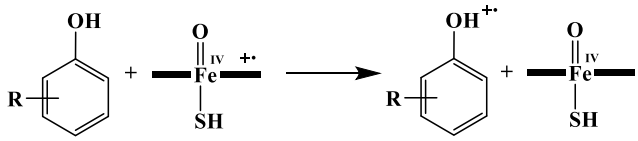

(1)

The free energy barriers of the outer-sphere ET ($\Delta G^{\neq}_{ET}$) can be appropriately estimated from the Marcus theory[71-73]. The Marcus theory relies on the transition-state formalism defining $\Delta G^{\neq}_{ET}$ in terms of two thermodynamic parameters, the free energy of reaction (ΔG_{ET}) and the reorganization energy (λ), as shown in eq. 2:

$$\Delta G^{\neq}_{ET} = \frac{\lambda}{4}\left(1 + \frac{\Delta G_{ET}}{\lambda}\right)^2 \quad (2)$$

The parameter λ consists of two parts, the solvent reorganization energy λ_0 and the inner reorganization energy λ_i, i.e. $\lambda = \lambda_i + \lambda_0$ (the details are shown in Section IV in the SI). Accordingly, **Table 1** shows the obtained reorganization energies, reaction energies and activation barriers for the ET reaction between triclosan and Cpd I of P450.

Table 1. The computed reorganization energies, free energies and activation barriers for the electron transfer from triclosan to Cpd I of P450 in both the HS and LS states

	λ_i (kcal/mol)	λ_0 (kcal/mol)	$\Delta G^{\neq}_{ET}$ (kcal/mol)	ΔG_{ET} (kcal/mol)
HS	9.7	7.8	54.4	44.1
LS	9.9	12.3	49.1	43.8

The obtained $\Delta G^{\neq}_{ET}$ is 54.4/49.1 kcal/mol for triclosan in the HS/LS states. The free-energy barriers are high (>20 kcal/mol), indicating that outer-sphere ET by P450 is unlikely for triclosan, consistent with the much higher IPs of this phenolic substrate than the spin-averaged electron affinities (EA) of only 2.9 eV for Cpd I of P450. Although this study only focused on the outer-sphere ET mechanism for triclosan, the results suggest that P450 is not able to catalyze

efficiently the oxidative phenol coupling by HRP-like peroxidation, partly because the spin-averaged EA of Cpd I of HRP (6.0 eV) approaches the IPs of diverse phenolic substrates (6.6−8.1 eV), including monophenols, bisphenols, polyphenols, alkylphenols and chlorophenols (**Table S20**), and is thus much higher than EA of 2.9 eV for Cpd I of P450.

Inner-Sphere Oxidation Mechanism

Free Energy Profiles for H-abstraction vs. O-addition. The free energy profiles for the inner-sphere oxidation pathways of triclosan catalyzed by Cpd I of P450 are shown in **Figure 1**, together with geometric details of the critical molecular species. The reactions start from reactant complexes ($^{4,2}RC_H$), in which the H-atom of the phenolic group of triclosan interacts with the iron-oxo moiety of Cpd I, existing in close-lying HS and LS spin states. $^{4,2}RC_H$ can traverse H-abstraction transition states $^{4,2}TS_H$ (confirmed by almost linear O•••H•••O angles and high imaginary frequencies), producing the intermediate complex $^{4,2}IM_H$ with the iron-hydroxo species (protonated Cpd II) and the phenoxy radical. And another pathway is O-addition onto the aromatic ring of triclosan. We find the H-abstraction pathway is the most favorable during inner-sphere oxidation of triclosan and by P450, as reflected in reaction barriers for O-addition at all unsubstituted aromatic carbons that are 21-27 kcal/mol higher than that for H-abstraction. This is in accordance with recent computational chemistry studies indicating that P450 GsfF performs phenolic O−H abstraction rather than O-addition during catalyzed oxidation of griseophenone B.[74] In the oxidation of triclosan, the dispersion energies lower the H-abstraction barriers by 1.5 kcal/mol, in accord with previous findings.[39,75]

Compared to toluene, an archetypical substrate for understanding regioselectivity in P450 chemistry, according to our calculations, the O-H BDE of triclosan (73.1 kcal/mol) is distinctly smaller than the C-H BDE of toluene (79.5 kcal/mol), indicating that H-abstraction is more likely

to occur for triclosan than for toluene. And even toluene oxidation gives mostly benzyl alcohol as H-abstraction product beyond cresol as O-addition product of the phenyl group.[76] We further computed the O-H BDEs for several other phenols such as monophenols, bisphenols, polyphenols, alkylphenols and chlorophenols (**Table S22**). The O-H BDEs for these diverse phenols are all within 68−74 kcal/mol, distinctly smaller than the C-H BDE of toluene, which suggests that P450-catalyzed H-abstraction is likely a common pathway during inner-sphere oxidation of phenols.

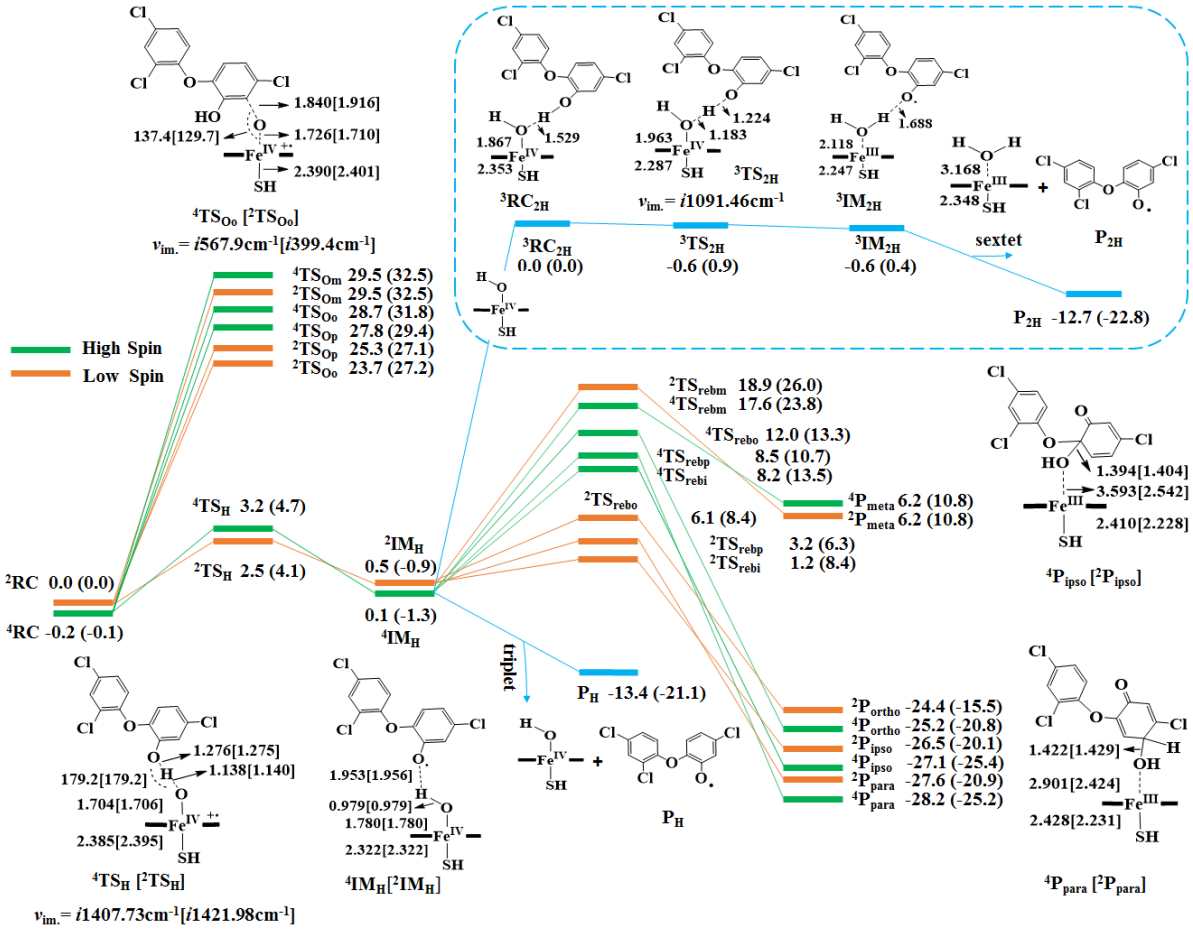

Figure 1. Free energy profiles for inner-sphere oxidation of triclosan by Cpd I of P450, along with the optimized geometries of the key reaction species in the HS and LS states. Free energies (kcal/mol) are relative to the doublet reactant complex ^{2}RC including dispersion corrections (no parentheses) and without dispersion (in parentheses). Geometrical parameters (lengths in Å and angles in degrees) are shown as the HS [LS] state. For the transition states, the imaginary frequencies are shown.

Two-State Reactivity Patterns in Hydroxylation. As shown in **Figure 1**, the intermediate complex $^{4,2}IM_H$ may lead to phenoxy radical rebound onto the hydroxo group of protonated Cpd II via its aromatic ring to yield the *ortho*-, *meta*-, *para*-, or *ipso*-addition quinol products in either spin state ($^{4,2}P_{ortho}$, $^{4,2}P_{meta}$, $^{4,2}P_{para}$ or $^{4,2}P_{ipso}$). The rebound reactions for the triclosan phenoxy radical at the *ortho*-, *para*- and *ipso*-carbon are highly exothermic, whereas the rebound reaction at the *meta*-carbon is highly endothermic. Considering the thermodynamically feasible rebound reactions, $^{2}IM_H$ encounters minor barriers of 0.7/5.6/2.7 kcal/mol for the triclosan phenoxy radical rebound onto the *ipso*/*ortho*/*para*-carbon. In contrast, we find that the rebound barriers of $^{4}IM_H$ onto corresponding aromatic carbons are typically 8−12 kcal/mol higher (or about 5−9 kcal/mol higher than the barriers of the H-abstraction steps). Accordingly, formation of the quinol intermediates mostly occurs in the LS state, which can further evolve into the hydroxylated products. Note that without dispersion effects, the phenoxy radical rebound steps in both spin states are rate-determining, but the dispersion energies lower the rebound barriers by 1-7 kcal/mol, whereas the LS rebound barriers of the triclosan radical at *ipso*-carbon, used to be called "essentially barrierless". However, regardless of this important dispersion contribution, the mechanism involving LS rebound is consistently more favorable than the HS rebound.

In the LS state, the barrier for rebound of the triclosan phenoxy radical at the *ipso*-carbon is 2.0 kcal/mol lower than the corresponding reaction at the *para*-carbon. When comparing the respective rate-determining steps, H-abstraction (2.5 kcal/mol) and radical rebound at the *para*-carbon (3.2 kcal/mol), considering a minor energy difference between $^{2}P_{ipso}$ and $^{2}P_{para}$, almost the same amount of quinols can be estimated. Accordingly, the most favorable quinol products formed in triclosan oxidation from both thermodynamical and kinetic considerations are expected to be $^{2}P_{para}$ and $^{2}P_{ipso}$. $^{2}P_{para}$ can further evolve into *para*-hydroxy-triclosan through

tautomerization with an exothermic reaction free energy of -22.8 kcal/mol (eq. 3), and $^{2}P_{ipso}$ can lead to 2,4-dichlorophenol with 4-chloroquinone through H-transfer and ether bond breaking, with an exothermic energy of -11.5 kcal/mol (eq. 4). Human P450 are known to catalyze hydroxylation of triclosan mainly at the *para*-position, with cleavage of the diphenyl ether bond at the *ipso*-position giving rise to *para*-hydroxy-triclosan, 2,4-dichlorophenol and 4-chlorocatechol, respectively.[69] The exothermic free energies of our reaction profiles explain these observations well.

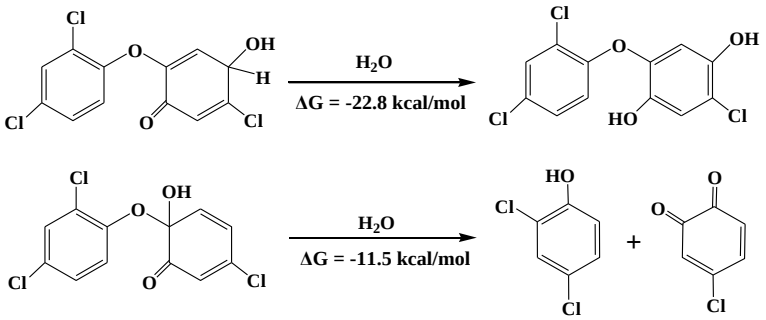

(3)

(4)

Secondary Phenolic H-Abstraction. Figure 1 also shows another pathway available to the $^{4,2}IM_H$ intermediates, whose conversion into ferryl-hydroxo species and a free triclosan radical is computed to be highly exothermic. Although their corresponding radical rebound reactions are more exothermic, under kinetic control we predict that the dissociation for $^{4}IM_H$ (but not $^{2}IM_H$) is more favorable than radical rebound with higher barriers, and we expect the radical species in the HS state can have large chance to detach. Note that the radical dissociation pathway has been shown to be prominent along with C−H hydroxylation by synthetic nonheme complexes (i.e. $Fe^{IV}O$, $Mn^{IV}O$, $Ru^{IV}O$ et. al.), while subsequent theoretical work has shown the rebound barrier is the key to determine the selectivity of radical rebound vs. radical dissociation.[35] Similarly, the triclosan phenoxy radical can leave the heme center unless other factors such as H-bonding prevent dissociation.

319 CYP158A1 and CYP158A2 have been shown to be able to catalyze the intermolecular
320 coupling of flaviolin in *Streptomyces coelicolor* A3(2), which are the only intermolecular
321 coupling enzymes with known three-dimensional structures in the presence of two phenolic
322 substrates in one pocket.[77,78] Until now, no P450 isoforms has been reported to be responsible for
323 phenol coupling of triclosan, we can make some hypothesis below. If the diradical coupling
324 mechanism works, in case with enough space in the P450 protein pocket, the distal triclosan
325 molecule may exchange with the proximal triclosan radical in the active site; Or in case that one
326 P450 protein pocket is not enough to accommodate two molecules, the triclosan radical may
327 leave the protein pocket and another triclosan molecule may enter into pocket near the heme
328 center. In both situations, the formed reactant complexes ($^3RC_{2H}$), can then undergo H-
329 abstraction from the phenolic group of triclosan by protonated Cpd II. As shown in the upright of
330 **Figure 1**, this H-abstraction from the phenolic group of triclosan by protonated Cpd II in the
331 ground triplet state is essentially barrierless and is exothermic by -12.7 kcal/mol, with formation
332 of the resting state of P450, and a triclosan phenoxy radical ready for radical collision.

333 **Regioselectivity for Phenol Coupling.** Considering the fate of phenoxy radicals involving
334 radical addition or diradical coupling to yield the C−C/C−O coupling products (O−O coupling
335 does not take place on account of the instability of the resultant peroxide), it is hard to obtain the
336 structures of all coupling products in experiments due to their structural heterogeneities.
337 However, the regioselectivity of phenol coupling is partially determined by the distribution of
338 unpaired electron spin in the radicals, with a high electron spin density at a particular site
339 indicating high reactivity.[79] As shown in **Figure 2**, for non-substituted positions, O22 and C15 of
340 the triclosan phenoxy radical are expected from this reasoning to be the two most reactive sites,
341 as they have the largest spin densities.

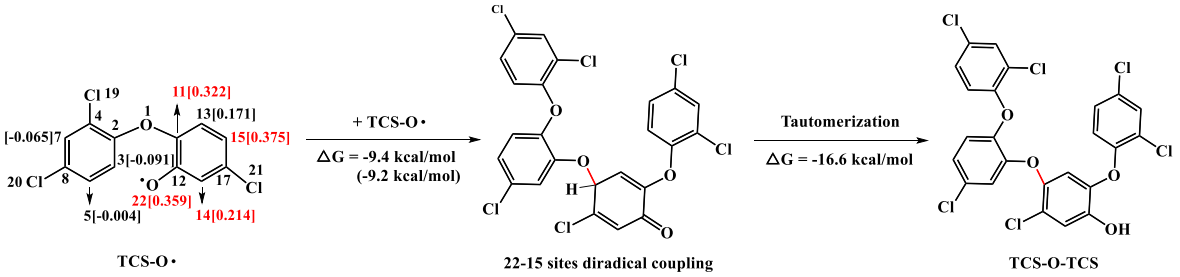

Figure 2. Spin densities for the triclosan phenoxy radical, and the most favorable diradical coupling reactions and subsequent tautomerization reactions with computed reaction free energies given (no parentheses: in polar environment; in parentheses: in non-polar environment).

We then speculate two possibilities, radical-addition or diradical coupling, for phenol coupling, dependent on the environment based on no available protein structural concerning phenol coupling of triclosan: 1) proximal triclosan radical addition to the distal neutral triclosan, or diradical coupling, happen in one P450 protein pocket (non-polar environment); 2) the phenoxy radical leaving the P450 pocket and reacting with another neutral phenol, or diradical coupling, happen in solution outside of the P450 pocket (polar environment). Thus, to further understand the linkage distributions during phenol coupling, a full study of the radical addition and diradical couplings in both polar and non-polar solution was performed. As shown in **Tables S24−S25**, all of the radical addition reactions are highly endothermic by 15−48 kcal/mol in polar and 20−38 kcal/mol non-polar environments, probably due to the low radical nature of the addition sites, and we thus focus on the diradical coupling reactions.

We studied the self-intermolecular coupling processes of triclosan phenoxy radical to form the dimeric intermediates, during which a total of 14 coupling reactions shown in **Tables S26−S27** were considered to encompass different linkages and identify the most stable stereoisomeric products. When analyzing these coupling reactions, C15−O22 (*para* C−O) coupling as shown in **Figure 2** emerges as the most likely coupling reaction with the most exothermic energy of -9.4 kcal/mol in the polar environment (-9.2 kcal/mol in the non-polar

environment), followed by C11−O22, C14−O22, C14−C14, C15−C15 and C15−C14 coupling reactions with exothermic energies from -7.5 to -2.9 kcal/mol in the polar environment (-7.1 to -2.8 kcal/mol in the non-polar environment); all other coupling reactions involving the C13 site are highly endothermic. These findings are very consistent with the spin density distributions on the triclosan phenoxy radical (C15 ≈ O22 > C14 >> C13). Note just six triclosan-O-triclosan metabolites were detected in mass spectra when triclosan was incubated with microsomes.[10]

Up to now, the favorable intermediates of radical coupling have been characterized. In most cases where the ring has lost aromaticity, the intermediates may undergo tautomerization to regain ring aromaticity in water solution. As shown in **Figure 2**, the energy of this tautomerization reaction is -16.6 kcal/mol for triclosan-O-triclosan formation in water solution. The results indicate that the tautomerization step is thermodynamically favorable, since barriers for hydrogen transfers through water bridging are small, and likely to yield the stable and fully aromatic products. Note that the constitutive androstane receptor (CAR) activity of triclosan-O-triclosan was reported to be about 7.2 times higher than that of triclosan.[10]

Fundamental Characteristics of Phenoxy Radical Rebound

Phenol Coupling vs. Phenol Hydroxylation. During P450-catalyzed alkane hydroxylation, the HS state may produce a radical with a significant barrier for rebound, although still much lower than that for the rate-determining H-abstraction step, whereas the LS state rebound is essentially barrierless.[31,33,34,36] Differently, oxidation of phenols such as triclosan, the real rebound transition states may be both on the HS and LS surfaces. The phenoxy radical rebound at some aromatic carbons in the LS state and at all aromatic carbons in the HS state are rate-determining. With high rebound barriers for phenoxy radicals at the thermodynamically feasible aromatic carbons, we propose a “two-state reactivity” as formulated in eq. 5 to eq. 7, which

reflect different rebound conditions. 1) When the LS rebound barrier is lower at least at one aromatic carbon and the HS rebound is higher than the H-abstraction barrier, most of the HS intermediates can proceed via the coupling pathway, while the LS species can mostly proceed to the hydroxylated products, giving the relative yield ratio [coupling]/[hydroxylation] of eq. 5 as simply the relative barriers of the HS and LS H-abstraction processes, since H-abstraction is the rate-determining step for both pathways. 2) When the barrier for LS rebound at all aromatic carbons is higher and the HS rebound barrier is distinctly higher than the H-abstraction barrier, the LS species can be subject to both hydroxylation and coupling, whereas the HS species can only proceed via coupling since the HS radical rebound is unfeasible; In this situation, as shown in eq. 6, the ratio of yields [coupling]/[hydroxylation] is approximately given by the relative barriers of the HS or LS H-abstraction (the lower one) and LS radical rebound steps, as these are the favorable rate-determining steps for coupling and hydroxylation pathways, respectively. 3) When both the LS and HS rebound steps have far higher barriers than the H-abstraction step, as shown in eq. 7, the LS and HS species can only proceed via the coupling pathway.

When $\Delta G^{\ddagger}_{LS\text{-}reb} < \Delta G^{\ddagger}_{LS\text{-}H}$ and $\Delta G^{\ddagger}_{HS\text{-}reb} > \Delta G^{\ddagger}_{HS\text{-}H}$:

$$[\text{Coupling}]/[\text{Hydroxylation}] \approx k_{HS\text{-}H}/k_{LS\text{-}H} \tag{5}$$

When $\Delta G^{\ddagger}_{LS\text{-}reb} > \Delta G^{\ddagger}_{LS\text{-}H}$ and $\Delta G^{\ddagger}_{HS\text{-}reb} >> \Delta G^{\ddagger}_{HS\text{-}H}$:

$$\begin{aligned} &[\text{Coupling}]/[\text{Hydroxylation}] \approx k_{HS\text{-}H}/k_{LS\text{-}reb} \text{ if } \Delta G^{\ddagger}_{HS\text{-}H} < \Delta G^{\ddagger}_{LS\text{-}H} \\ &[\text{Coupling}]/[\text{Hydroxylation}] \approx k_{LS\text{-}H}/k_{LS\text{-}reb} \text{ if } \Delta G^{\ddagger}_{HS\text{-}H} > \Delta G^{\ddagger}_{LS\text{-}H} \end{aligned} \tag{6}$$

When $\Delta G^{\ddagger}_{LS\text{-}reb} >> \Delta G^{\ddagger}_{LS\text{-}H}$ and $\Delta G^{\ddagger}_{HS\text{-}reb} >> \Delta G^{\ddagger}_{HS\text{-}H}$:

$$[\text{Coupling}]/[\text{Hydroxylation}] \approx \infty \tag{7}$$

Based on the data provided in **Figure 1**, oxidation of triclosan by P450 fits well into the situation of eq. 5. According to the model, we can estimate the ratio [coupling]/[hydroxylation] using the Eyring equation (eq. 8) as roughly 1:4 for oxidation of triclosan ($\Delta G^{\ddagger}_{HS\text{-}H} - \Delta G^{\ddagger}_{LS\text{-}H} =$ 0.8 kcal/mol), which implies that the phenol hydroxylation is favorable for oxidation of triclosan.

$$k = \frac{k_B T}{h} \cdot \frac{1}{c^0} \exp\left(-\frac{\Delta G^{\ddagger}}{RT}\right) \quad (8)$$

k: reaction rate constant; k_B: Boltzmann constant; h: Planck constant; R: gas constant; T: temperature in Kelvin; c^0: concentration defining the standard state (typically 1 mol/L).

This model largely explains the experimental ratios of the reaction rates of hydroxylation vs. coupling in the range of (1.5-17):1 for triclosan incubated in human microsomes.[10] In order to further limit the effect of molecular specificity on phenol coupling mechanism obtained from triclosan, we extended the study on the phenol coupling mechanism of 3-chloro-bisphenol A (3-ClBPA), as the free energy profiles shown in **Figure S5**. It shows that 3-ClBPA resembles well the phenol coupling mechanism of triclosan that a diradical pathway is successively facilitated by Cpd I and protonated Cpd II of P450, thus we can estimate its ratio [coupling]/[hydroxylation] as roughly 1:2 via eq. 5 and eq. 8. This result is in consistent with that 3-ClBPA-O-3-ClBPA is a significant metabolite from 3-ClBPA incubated by P450 in experiment.[10]

Origin of the High Rebound Barrier for Phenoxy Radicals. As the spin densities show in **Table S3**, the intermediate complexes ($^{4,2}IM_H$) of the triclosan consist of an iron-hydroxo group ($PorFe^{IV}OH$) with a closed-shell porphyrin and a nearby phenoxy radical (electronic configuration: $\delta_{x^2-y^2}{}^2\pi^*_{xz}{}^1\pi^*_{yz}{}^1a_{2u}{}^2\phi_{Rad}{}^1$). In the subsequent phenoxy radical rebound leading to the iron-quinol species, the electron from the phenoxy radical shifts onto the low-lying orbitals (π^*_{xz}) in the LS state, while the HS process involves the electron shifting onto the high-lying $\sigma^*_{z^2}$

orbital to conserve the HS state, with elongation of the Fe-O and Fe-S bond lengths in the quinol products (**Figure 1**). Previous studies on alkane hydroxylation mechanisms catalyzed by P450 have indicated that the HS rebound barriers for the alkyl radicals are 1−5 kcal/mol, owing to the excitation energy to the σ^*z^2 orbital.[31,32,34,40,41] This electron excitation partly contributes to the high HS rebound barrier of the phenoxy radical, but is not enough to cause the HS rebound barrier more than 8 kcal/mol and even a significant rebound barriers in the LS state.

Table 2. The calculated spin delocalization ratios, SOMOs and IPs for diverse phenoxy and alkylbenzene radicals

Radical	Spin Delocalization Ratio (%)	SOMO (eV)	Radical	Spin Delocalization Ratio (%)	SOMO (eV)
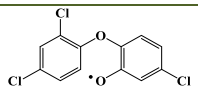	61	-0.23	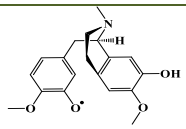	63	-0.20
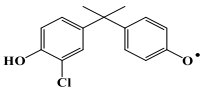	57	-0.22	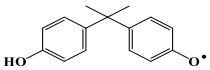	57	-0.22
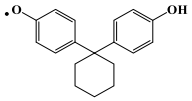	58	-0.21	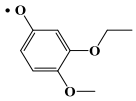	62	-0.20
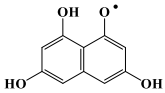	62	-0.19	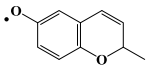	64	-0.19
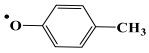	58	-0.22	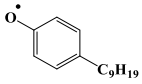	61	-0.22
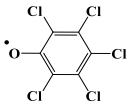	64	-0.25	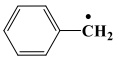	22	-0.18
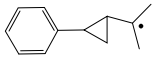	4	-0.17	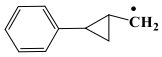	2	-0.17
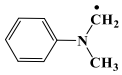	18	-0.14	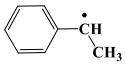	23	-0.17
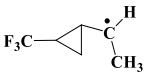	3	-0.18		4	-0.16

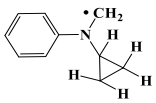	17	-0.14	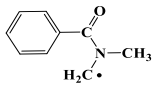	23	-0.17

As shown in **Table 2**, the radical spin formed initially on the hydroxyl oxygen can readily delocalize into the aromatic ring (58%−64%) in monophenols, bisphenols, polyphenols, alkylphenols and chlorophenols, while little spin delocalization occurs for several common alkylbenzene radicals (2%−23%). Spin delocalization may result in lower electron donor ability of the phenoxy radicals, as reflected in **Table 2** by the significantly lower energies of the singly occupied molecular orbitals (SOMOs) of phenoxy radicals in the range from -0.25 to -0.19 eV, compared to alkylbenzene radicals (between -0.18 and -0.14 eV). Thus, another factor leading to the high rebound barriers in phenol coupling by P450 could be the low electron donor ability of the phenoxy radicals. In order to further understand this, we compared the computed HS rebound barrier heights (B3LYP/BSI level with free energy correction, **Table S32**) with the phenolic radical IPs (**Table S33** as shown in **Figure 3**. The trend demonstrates an increase of rebound barrier heights with increasing phenolic radical IPs, which strongly suggests that when the phenoxy radical center becomes a weaker electron donor (higher IP), the rebound barrier increases. Considering the very strong correlation, we conclude that the electron donor ability of the phenoxy radicals is the main factor determining the barrier height of rebound, and this physical model for P450 rebound reactivity may be of substantial use in many other contexts of P450 chemistry.

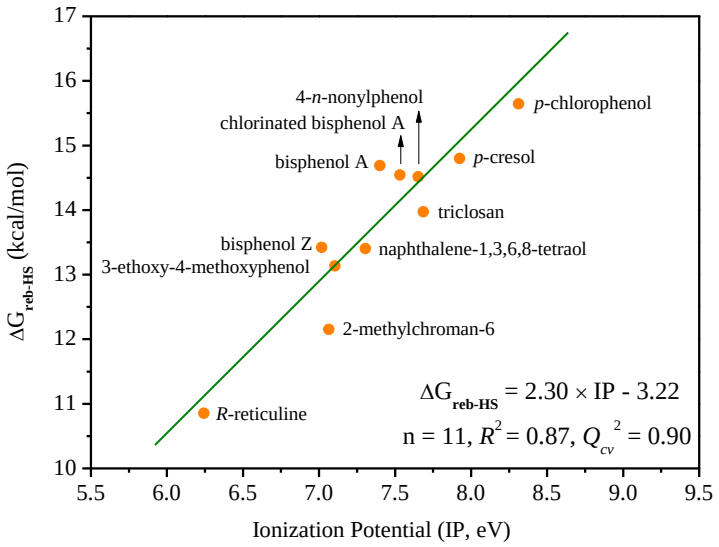

Figure 3. Correlation of rebound barrier heights in the HS state with the IPs of diverse phenolic radicals

Environmental Implications

Most emerging pollutants proceed through the biotransformation processes, especially by P450 enzymes, which may produce metabolites with altering environmental behavior and toxicological profile. Especially, it has been found that as the number of aromatic rings increase, there is a concomitant increase in lipophilicity of the compounds,[80] resulting in potentially higher toxicity, and thus the biotransformation involving coupling reactions of emerging phenolic pollutants has important environmental significance. Understanding the biotransformation mechanisms of emerging pollutants such as phenol coupling to develop mechanism-based methods for screening of metabolites will undoubtedly improve the efficiency of metabolites-oriented analysis in environmental risk assessment. As the mechanism revealed in this work, aromatic delocalization is arguably the decisive factor that lowers the electron donor ability of triclosan phenoxy radical and enables radical dissociation and self-coupling reaction catalyzed by P450 enzymes. Furthermore, aromatic delocalization as an intrinsic nature for most phenolic

471 pollutants (**Table 2**), which can endow the phenoxy radical sufficient lifetime during P450-
472 mediated reactions, thus the phenol coupling reactions have great chance to happen between
473 different phenolic pollutants when they co-exposure to the biotransformation system. As more
474 attention has been paid in the joint metabolic effect of multiple environmental chemicals
475 recently,[81] our proposed phenol coupling mechanism can be helpful to screen the possible cross-
476 coupling metabolites between different phenolic pollutants, as a leading step of experiments.

477 Aromatic delocalization is a common feature also of other radicals of aromatic pollutants,
478 i.e. benzenamino radicals, thiophenoxy radicals, and phenylphosphine radicals (for example, the
479 spin delocalization ratio is 55% for 2,6-$(CH_3)_2C_6H_3NH$•, 70% for C_6H_5S•, and 87% for
480 C_6H_5PH•), and thus we predict that they may undergo coupling reactions as well. P450-catalyzed
481 coupling of norharman and aniline has been reported, and this coupling product can be further
482 oxidized into a mutagenic hydroxylamine.[82] However, it is difficult to propose a reaction product
483 of either norharman or aniline that is stable enough to migrate from the P450 and reactive
484 enough to couple with aniline, or *vice versa*. The phenol coupling mechanism proposed in this
485 work provides a simple rationale for this disputed coupling mechanism. The free energy profile
486 for the reaction of norharman catalyzed by Cpd I of P450 is displayed in **Figure S6**, specially
487 showing much higher rebound barriers for the norharman amino radical than for H-abstraction in
488 the HS state to lead to aromatic hydroxylation and the N-hydroxylation products. In contrast, the
489 rebound barriers for the norharman amino radical at the aromatic ring in the LS state are slightly
490 lower than for H-abstraction; this situation is importantly covered by our model's first scenario,
491 eq. 5, where the HS H-abstraction (leading to coupling) is more favorable than the LS
492 counterpart (leading to hydroxylation), and the model can thus explain the observation of
493 coupling products upon oxidation of norharman. In both norharman and aniline amino radicals,

about 50% and 40% radical spin delocalizes into the aromatic rings from the amino nitrogen. Aromatic delocalization in amino radicals may produce large radical rebound barriers, further facilitating radical dissociation and coupling reaction. We hope that the fundamental mechanism described in this work will aid the high-throughput screening of putative metabolites of aromatic pollutants in toxicological assays, in particular considering the probable overlooked importance of many of these metabolites.

ASSOCIATED CONTENT

Supporting Information. Optimized structures of the molecular species involved in P450-catalyzed triclosan pathway optimized at the B3LYP/BSII level; Evaluation of the solvation effect in P450-catalyzed triclosan pathway with SMD solvation model; Details for quantum chemical cluster calculations; Estimation of activation barriers for electron transfer processes by Marcus theory; Potential energy profiles for P450-catalyzed 3-chloro-bisphenol A pathway; Potential energy profiles for P450-catalyzed norharman pathway; Mulliken spin densities and charges; Energies for all molecular species; Cartesian coordinates of all structures. This material is available free of charge via the Internet at http://pubs.acs.org.

AUTHOR INFORMATION

Corresponding Author

**(L.J.) E-mail: jilienv@zju.edu.cn

Author Contributions

‡F. G. and L. C. contribute equally to this work.

Notes

The authors declare no competing financial interest.

ACKNOWLEDGMENT

This work was supported by the National Natural Science Foundation of China (No. 21677125) and Japan Society for the Promotion of Science (No. 19524). The China National Supercomputing Center in Shenzhen is acknowledged for providing the computing resources.

REFERENCES

(1) Tang, M. C.; Zou, Y.; Watanabe, K.; Walsh, C. T.; Tang, Y. Oxidative cyclization in natural product biosynthesis. *Chem. Rev.* **2017,** *117* (8), 5226-5333.

(2) Mizutani, M.; Sato, F. Unusual p450 reactions in plant secondary metabolism. *Arch. Biochem. Biophys.* **2011,** *507* (1), 194-203.

(3) Woithe, K.; Geib, N.; Zerbe, K.; Li, D. B.; Heck, M.; Fournier-Rousset, S.; Meyer, O.; Vitali, F.; Matoba, N.; Abou-Hadeed, K.; Robinson, J. A. Oxidative phenol coupling reactions catalyzed by oxyb: A cytochrome p450 from the vancomycin producing organism. Implications for vancomycin biosynthesis. *J. Am. Chem. Soc.* **2007,** *129* (21), 6887-6895.

(4) Guengerich, F. P. Common and uncommon cytochrome p450 reactions related to metabolism and chemical toxicity. *Chem. Res. Toxicol.* **2001,** *14* (6), 611-650.

(5) Liu, R. Z.; Song, S. J.; Lin, Y. F.; Ruan, T.; Jiang, G. B. Occurrence of synthetic phenolic antioxidants and major metabolites in municipal sewage sludge in china. *Environ. Sci. Technol.* **2015,** *49* (4), 2073-2080.

536 (6) Wang, W.; Asimakopoulos, A. G.; Abualnaja, K. O.; Covaci, A.; Gevao, B.; Johnson-
537 Restrepo, B.; Kumosani, T. A.; Malarvannan, G.; Minh, T. B.; Moon, H. B.; Nakata, H.; Sinha,
538 R. K.; Kannan, K. Synthetic phenolic antioxidants and their metabolites in indoor dust from
539 homes and microenvironments. *Environ. Sci. Technol.* **2016,** *50* (1), 428-434.

540 (7) Mizukawa, H.; Nomiyama, K.; Nakatsu, S.; Yamamoto, M.; Ishizuka, M.; Ikenaka, Y.;
541 Nakayama, S. M. M.; Tanabe, S. Anthropogenic and naturally produced brominated phenols in
542 pet blood and pet food in japan. *Environ. Sci. Technol.* **2017,** *51* (19), 11354-11362.

543 (8) Wang, X. Y.; Hou, X. W.; Zhou, Q. F.; Liao, C. Y.; Jiang, G. B. Synthetic phenolic
544 antioxidants and their metabolites in sediments from the coastal area of northern china: Spatial
545 and vertical distributions. *Environ. Sci. Technol.* **2018,** *52* (23), 13690-13697.

546 (9) Wang, X. Y.; Hou, X. W.; Hu, Y.; Zhou, Q. F.; Liao, C. Y.; Jiang, G. B. Synthetic
547 phenolic antioxidants and their metabolites in mollusks from the chinese bohai sea: Occurrence,
548 temporal trend, and human exposure. *Environ. Sci. Technol.* **2018,** *52* (17), 10124-10133.

549 (10) Ashrap, P.; Zheng, G. M.; Wan, Y.; Li, T.; Hu, W. X.; Li, W. J.; Zhang, H.; Zhang, Z. B.;
550 Hu, J. Y. Discovery of a widespread metabolic pathway within and among phenolic xenobiotics.
551 *Proc. Natl. Acad. Sci. U. S. A.* **2017,** *114* (23), 6062-6067.

552 (11) Barton, D. H. R.; Cohen, T., Some biogenetic aspects of phenol oxidation. In *Festschrift*
553 *prof. Dr. Arthur stoll*, Birkhauser Verlag: Basel, 1957; p 117−144.

554 (12) Rittle, J.; Green, M. T. Cytochrome p450 compound i: Capture, characterization, and c-h
555 bond activation kinetics. *Science* **2010,** *330* (6006), 933-937.

556 (13) Mittra, K.; Green, M. T. Reduction potentials of p450 compounds i and ii: Insight into the
557 thermodynamics of c-h bond activation. *J. Am. Chem. Soc.* **2019,** *141* (13), 5504-5510.

558 (14) Grobe, N.; Zhang, B.; Fisinger, U.; Kutchan, T. M.; Zenk, M. H.; Guengerich, F. P.
559 Mammalian cytochrome p450 enzymes catalyze the phenol-coupling step in endogenous
560 morphine biosynthesis. *J. Biol. Chem.* **2009,** *284* (36), 24425-24431.

561 (15) Belin, P.; Le Du, M. H.; Fielding, A.; Lequin, O.; Jacquet, M.; Charbonnier, J.-B.; Lecoq,
562 A.; Thai, R.; Courcon, M.; Masson, C.; Dugave, C.; Genet, R.; Pernodet, J.-L.; Gondry, M.
563 Identification and structural basis of the reaction catalyzed by cyp121, an essential cytochrome
564 p450 in mycobacterium tuberculosis. *Proc. Natl. Acad. Sci. U. S. A.* **2009,** *106* (18), 7426-7431.

565 (16) Ohe, T.; Mashino, T.; Hirobe, M. Substituent elimination from *p*-substituted phenols by
566 cytochrome p450. *Ipso*-substitution by the oxygen atom of the active species. *Drug Metab.*
567 *Dispos.* **1997,** *25* (1), 116-122.

568 (17) Sarabia, S. F.; Zhu, B. T.; Kurosawa, T.; Tohma, M.; Liehr, J. G. Mechanism of
569 cytochrome p450-catalyzed aromatic hydroxylation of estrogens. *Chem. Res. Toxicol.* **1997,** *10*
570 (7), 767-771.

571 (18) Stresser, D. M.; Kupfer, D. Catalytic characteristics of cyp3a4: Requirement for a
572 phenolic function in ortho hydroxylation of estradiol and mono-o-demethylated methoxychlor.
573 *Biochemistry* **1997,** *36* (8), 2203-2210.

574 (19) Ehlting, J.; Hamberger, B.; Million-Rousseau, R.; Werck-Reichhart, D. Cytochromes
575 p450 in phenolic metabolism. *Phytochem. Rev.* **2006,** *5* (2-3), 239-270.

576 (20) Sono, M.; Roach, M. P.; Coulter, E. D.; Dawson, J. H. Heme-containing oxygenases.
577 *Chem. Rev.* **1996,** *96* (7), 2841-2887.

578 (21) Poulos, T. L., In *The porphyrin handbook*, 2000; Vol. 4, pp 189-218.

579 (22) Dawson, J. H. Probing structure-function relations in heme-containing oxygenases and
580 peroxidases. *Science* **1988,** *240* (4851), 433-439.

581 (23) Berglund, G. I.; Carlsson, G. H.; Smith, A. T.; Szoke, H.; Henriksen, A.; Hajdu, J. The
582 catalytic pathway of horseradish peroxidase at high resolution. *Nature* **2002,** *417* (6887), 463-
583 468.

584 (24) de Visser, S. P.; Shaik, S.; Sharma, P. K.; Kumar, D.; Thiel, W. Active species of
585 horseradish peroxidase (hrp) and cytochrome p450: Two electronic chameleons. *J. Am. Chem.*
586 *Soc.* **2003,** *125* (51), 15779-15788.

587 (25) Meyer, A. H.; Dybala-Defratyka, A.; Alaimo, P. J.; Geronimo, I.; Sanchez, A. D.; Cramer,
588 C. J.; Elsner, M. Cytochrome p450-catalyzed dealkylation of atrazine by rhodococcus sp. Strain
589 ni86/21 involves hydrogen atom transfer rather than single electron transfer. *Dalton Trans* **2014,**
590 *43* (32), 12175-12186.

591 (26) Li, Y.; Shi, X.; Zhang, Q.; Hu, J.; Chen, J.; Wang, W. Computational evidence for the
592 detoxifying mechanism of epsilon class glutathione transferase toward the insecticide ddt.
593 *Environ. Sci. Technol.* **2014,** *48* (9), 5008-5016.

594 (27) Sadowsky, D.; McNeill, K.; Cramer, C. J. Dehalogenation of aromatics by nucleophilic
595 aromatic substitution. *Environ. Sci. Technol.* **2014,** *48* (18), 10904-10911.

596 (28) Krzeminska, A.; Paneth, P. Dft studies of sn2 dechlorination of polychlorinated biphenyls.
597 *Environ. Sci. Technol.* **2016,** *50* (12), 6293-6298.

598 (29) Pati, S. G.; Kohler, H. P.; Pabis, A.; Paneth, P.; Parales, R. E.; Hofstetter, T. B. Substrate
599 and enzyme specificity of the kinetic isotope effects associated with the dioxygenation of
600 nitroaromatic contaminants. *Environ. Sci. Technol.* **2016,** *50* (13), 6708-6716.

601 (30) Fu, Z. Q.; Wang, Y.; Chen, J. W.; Wang, Z. Y.; Wang, X. B. How pbdes are transformed
602 into dihydroxylated and dioxin metabolites catalyzed by the active center of cytochrome p450s:
603 A dft study. *Environ. Sci. Technol.* **2016,** *50* (15), 8155-8163.

604 (31) Ogliaro, F.; Harris, N.; Cohen, S.; Filatov, M.; de Visser, S. P.; Shaik, S. A model
605 "rebound" mechanism of hydroxylation by cytochrome p450: Stepwise and effectively concerted
606 pathways, and their reactivity patterns. *J. Am. Chem. Soc.* **2000,** *122* (37), 8977-8989.

607 (32) Yoshizawa, K.; Kamachi, T.; Shiota, Y. A theoretical study of the dynamic behavior of
608 alkane hydroxylation by a compound i model of cytochrome p450. *J. Am. Chem. Soc.* **2001,** *123*
609 (40), 9806-9816.

610 (33) Shaik, S.; Cohen, S.; Wang, Y.; Chen, H.; Kumar, D.; Thiel, W. P450 enzymes: Their
611 structure, reactivity, and selectivity-modeled by qm/mm calculations. *Chem. Rev.* **2010,** *110* (2),
612 949-1017.

613 (34) Shaik, S.; Kumar, D.; de Visser, S. P. Valence bond modeling of trends in hydrogen
614 abstraction barriers and transition states of hydroxylation reactions catalyzed by cytochrome
615 p450 enzymes. *J. Am. Chem. Soc.* **2008,** *130* (31), 10128-10140.

616 (35) Cho, K. B.; Hirao, H.; Shaik, S.; Nam, W. To rebound or dissociate? This is the
617 mechanistic question in c-h hydroxylation by heme and nonheme metal-oxo complexes. *Chem.*
618 *Soc. Rev.* **2016,** *45* (5), 1197-1210.

619 (36) Shaik, S.; Kumar, D.; de Visser, S. P.; Altun, A.; Thiel, W. Theoretical perspective on the
620 structure and mechanism of cytochrome p450 enzymes. *Chem. Rev.* **2005,** *105* (6), 2279-2328.

621 (37) de Visser, S. P.; Ogliaro, F.; Shaik, S. How does ethene inactivate cytochrome p450 en
622 route to its epoxidation? A density functional study. *Angewandte Chemie-International Edition*
623 **2001,** *40* (15), 2871-2874.

624 (38) Ji, L.; Schuurmann, G. Computational evidence for alpha-nitrosamino radical as initial
625 metabolite for both the p450 dealkylation and denitrosation of carcinogenic nitrosamines. *J. Phys.*
626 *Chem. B* **2012,** *116* (2), 903-912.

627 (39) Ji, L.; Faponle, A. S.; Quesne, M. G.; Sainna, M. A.; Zhang, J.; Franke, A.; Kumar, D.;
628 van Eldik, R.; Liu, W. P.; de Visser, S. P. Drug metabolism by cytochrome p450 enzymes: What
629 distinguishes the pathways leading to substrate hydroxylation over desaturation? *Chem. Eur. J.*
630 **2015,** *21* (25), 9083-9092.

631 (40) de Visser, S. P.; Ogliaro, F.; Sharma, P. K.; Shaik, S. What factors affect the
632 regioselectivity of oxidation by cytochrome p450? A dft study of allylic hydroxylation and
633 double bond epoxidation in a model reaction. *J. Am. Chem. Soc.* **2002,** *124* (39), 11809-11826.

634 (41) Shaik, S.; Cohen, S.; de Visser, S. P.; Sharma, P. K.; Kumar, D.; Kozuch, S.; Ogliaro, F.;
635 Danovich, D. The "rebound controversy": An overview and theoretical modeling of the rebound
636 step in c-h hydroxylation by cytochrome p450. *Eur. J. Inorg. Chem.* **2004,** (2), 207-226.

637 (42) Company, A.; Prat, I.; Frisch, J. R.; Mas-Balleste, R.; Gueell, M.; Juhasz, G.; Ribas, X.;
638 Muenck, E.; Luis, J. M.; Que, L., Jr.; Costas, M. Modeling the cis-oxo-labile binding site motif
639 of non-heme iron oxygenases: Water exchange and oxidation reactivity of a non-heme iron(iv)-
640 oxo compound bearing a tripodal tetradentate ligand. *Chem. Eur. J.* **2011,** *17* (5), 1622-1634.

641 (43) Janardanan, D.; Usharani, D.; Chen, H.; Shaik, S. Modeling c-h abstraction reactivity of
642 nonheme fe(iv)o oxidants with alkanes: What role do counter ions play? *J. Phys. Chem. Lett.*
643 **2011,** *2* (20), 2610-2617.

644 (44) Cho, K.-B.; Shaik, S.; Nam, W. Theoretical investigations into c-h bond activation
645 reaction by nonheme mn(iv)o complexes: Multistate reactivity with no oxygen rebound. *J. Phys.*
646 *Chem. Lett.* **2012,** *3* (19), 2851-2856.

647 (45) Cho, K. B.; Wu, X.; Lee, Y. M.; Kwon, Y. H.; Shaik, S.; Nam, W. Evidence for an
648 alternative to the oxygen rebound mechanism in c-h bond activation by non-heme fe(iv)o
649 complexes. *J. Am. Chem. Soc.* **2012,** *134* (50), 20222-20225.

650 (46) Ji, L.; Ji, S.; Wang, C.; Kepp, K. P. Molecular mechanism of alternative p450-catalyzed
651 metabolism of environmental phenolic endocrine-disrupting chemicals. *Environ. Sci. Technol.*
652 **2018,** *52* (7), 4422-4431.

653 (47) Schyman, P.; Lai, W.; Chen, H.; Wang, Y.; Shaik, S. The directive of the protein: How
654 does cytochrome p450 select the mechanism of dopamine formation? *J. Am. Chem. Soc.* **2011,**
655 *133* (20), 7977-7984.

656 (48) Ji, L.; Schuurmann, G. Model and mechanism: N-hydroxylation of primary aromatic
657 amines by cytochrome p450. *Angew. Chem. Int. Ed.* **2013,** *52* (2), 744-748.

(49) Zhang, Q.; Ji, S.; Chai, L.; Yang, F.; Zhao, M.; Liu, W.; Schueuermann, G.; Ji, L. Metabolic mechanism of aryl phosphorus flame retardants by cytochromes p450: A combined experimental and computational study on triphenyl phosphate. *Environ. Sci. Technol.* **2018,** *52* (24), 14411-14421.

(50) Lee, C. T.; Yang, W. T.; Parr, R. G. Development of the colle-salvetti correlation-energy formula into a functional of the electron-density. *Phys. Rev. B: Condens. Matter Mater. Phys.* **1988,** *37* (2), 785-789.

(51) Becke, A. D. Density-functional thermochemistry. Iii. The role of exact exchange. *J. Chem. Phys.* **1993,** *98* (7), 5648-5652.

(52) Hay, P. J.; Wadt, W. R. Abinitio effective core potentials for molecular calculations - potentials for the transition-metal atoms sc to hg. *J. Chem. Phys.* **1985,** *82* (1), 270-283.

(53) Kumar, D.; de Visser, S. P.; Shaik, S. How does product isotope effect prove the operation of a two-state "rebound" mechanism in c-h hydroxylation by cytochrome p450? *J. Am. Chem. Soc.* **2003,** *125* (43), 13024-13025.

(54) Porro, C. S.; Kumar, D.; de Visser, S. P. Electronic properties of pentacoordinated heme complexes in cytochrome p450 enzymes: Search for an fe(i) oxidation state. *Phys. Chem. Chem. Phys.* **2009,** *11* (43), 10219-10226.

(55) Strickland, N.; Harvey, J. N. Spin-forbidden ligand binding to the ferrous-heme group: Ab initio and dft studies. *J. Phys. Chem. B* **2007,** *111* (4), 841-852.

(56) Altun, A.; Breidung, J.; Neese, F.; Thiel, W. Correlated ab initio and density functional studies on h2 activation by feo^{+}. *J. Chem. Theory Comput.* **2014,** *10* (9), 3807-3820.

(57) Tao, J.; Perdew, J. P.; Staroverov, V. N.; Scuseria, G. E. Climbing the density functional ladder: Nonempirical meta-generalized gradient approximation designed for molecules and solids. *Phys. Rev. Lett.* **2003,** *91* (14), 146401.

(58) Staroverov, V. N.; Scuseria, G. E.; Tao, J. M.; Perdew, J. P. Comparative assessment of a new nonempirical density functional: Molecules and hydrogen-bonded complexes. *J. Chem. Phys.* **2003,** *119* (23), 12129-12137.

(59) Perdew, J. P.; Wang, Y. Accurate and simple analytic representation of the electron-gas correlation energy. *Phys. Rev. B: Condens. Matter Mater. Phys.* **1992,** *45* (23), 13244-13249.

(60) Becke, A. D. Density-functional exchange-energy approximation with correct asymptotic-behavior. *Phys. Rev. A: At., Mol., Opt. Phys.* **1988,** *38* (6), 3098-3100.

(61) Adamo, C.; Barone, V. Exchange functionals with improved long-range behavior and adiabatic connection methods without adjustable parameters: The mpw and mpw1pw models. *J. Chem. Phys.* **1998,** *108* (2), 664-675.

(62) Zhao, Y.; Truhlar, D. G. A new local density functional for main-group thermochemistry, transition metal bonding, thermochemical kinetics, and noncovalent interactions. *J. Chem. Phys.* **2006,** *125* (19), 194101.

(63) Miertus, S.; Scrocco, E.; Tomasi, J. Electrostatic interaction of a solute with a continuum - a direct utilization of abinitio molecular potentials for the prevision of solvent effects. *Chem. Phys.* **1981,** *55* (1), 117-129.

698 (64) Ogliaro, F.; de Visser, S. P.; Cohen, S.; Kaneti, J.; Shaik, S. The experimentally elusive
699 oxidant of cytochrome p450: A theoretical "trapping" defining more closely the "real" species.
700 *ChemBioChem* **2001,** *2* (11), 848-851.

701 (65) Marenich, A. V.; Cramer, C. J.; Truhlar, D. G. Universal solvation model based on solute
702 electron density and on a continuum model of the solvent defined by the bulk dielectric constant
703 and atomic surface tensions. *J. Phys. Chem. B* **2009,** *113* (18), 6378-6396.

704 (66) Grimme, S. Semiempirical gga-type density functional constructed with a long-range
705 dispersion correction. *J. Comput. Chem.* **2006,** *27* (15), 1787-1799.

706 (67) Himo, F. Recent trends in quantum chemical modeling of enzymatic reactions. *J. Am.*
707 *Chem. Soc.* **2017,** *139* (20), 6780-6786.

708 (68) Senn, H. M.; Thiel, W. Qm/mm methods for biomolecular systems. *Angew. Chem. Int.*
709 *Ed. Engl.* **2009,** *48* (7), 1198-1229.

710 (69) Wu, Y. F.; Chitranshi, P.; Loukotkova, L.; da Costa, G. G.; Beland, F. A.; Zhang, J.;
711 Fang, J. L. Cytochrome p450-mediated metabolism of triclosan attenuates its cytotoxicity in
712 hepatic cells. *Arch. Toxicol.* **2017,** *91* (6), 2405-2423.

713 (70) Frisch, M. J.; Trucks, G. W.; Schlegel, H. B.; Scuseria, G. E.; Robb, M. A.; Cheeseman, J.
714 R.; Scalmani, G.; Barone, V.; Mennucci, B.; Petersson, G. A.; Nakatsuji, H.; Caricato, M.; Li, X.;
715 Hratchian, H. P.; Izmaylov, A. F.; Bloino, J.; Zheng, G.; Sonnenberg, J. L.; Hada, M.; Ehara, M.;
716 Toyota, K.; Fukuda, R.; Hasegawa, J.; Ishida, M.; Nakajima, T.; Honda, Y.; Kitao, O.; Nakai, H.;
717 Vreven, T.; Montgomery, J. A.; Jr.; Peralta, J. E.; Ogliaro, F.; Bearpark, M.; Heyd, J. J.; Brothers,
718 E.; Kudin, K. N.; Staroverov, V. N.; Kobayashi, R.; Normand, J.; Raghavachari, K.; Rendell, A.;

Burant, J. C.; Iyengar, S. S.; Tomasi, J.; Cossi, M.; Rega, N.; Millam, N. J.; Klene, M.; Knox, J. E.; Cross, J. B.; Bakken, V.; Adamo, C.; Jaramillo, J.; Gomperts, R.; Stratmann, R. E.; Yazyev, O.; Austin, A. J.; Cammi, R.; Pomelli, C.; Ochterski, J. W.; Martin, R. L.; Morokuma, K.; Zakrzewski, V. G.; Voth, G. A.; Salvador, P.; Dannenberg, J. J.; Dapprich, S.; Daniels, A. D.; Farkas, Ö.; Foresman, J. B.; Ortiz, J. V.; Cioslowski, J.; Fox, D. J. Gaussian, Inc.: Wallingford CT, 2013. Gaussian 09, Revision D.01.

(71) Marcus, R. A. Electron-transfer reactions in chemistry - theory and experiment (nobel lecture). *Angew. Chem. Int. Ed.* **1993,** *32* (8), 1111-1121.

(72) Jones, G. O.; Liu, P.; Houk, K. N.; Buchwald, S. L. Computational explorations of mechanisms and ligand-directed selectivities of copper-catalyzed ullmann-type reactions. *J. Am. Chem. Soc.* **2010,** *132* (17), 6205-6213.

(73) Lin, C. Y.; Coote, M. L.; Gennaro, A.; Matyjaszewski, K. Ab initio evaluation of the thermodynamic and electrochemical properties of alkyl halides and radicals and their mechanistic implications for atom transfer radical polymerization. *J. Am. Chem. Soc.* **2008,** *130* (38), 12762-12774.

(74) Grandner, J. M.; Cacho, R. A.; Tang, Y.; Houk, K. N. Mechanism of the p450-catalyzed oxidative cyclization in the biosynthesis of griseofulvin. *ACS Catal.* **2016,** *6* (7), 4506-4511.

(75) Lonsdale, R.; Harvey, J. N.; Mulholland, A. J. Inclusion of dispersion effects significantly improves accuracy of calculated reaction barriers for cytochrome p450 catalyzed reactions. *J. Phys. Chem. Lett.* **2010,** *1* (21), 3232-3237.

739 (76) Tassaneeyakul, W.; Birkett, D. J.; Edwards, J. W.; Veronese, M. E.; Tassaneeyakul, W.;
740 Tukey, R. H.; Miners, J. O. Human cytochrome p450 isoform specificity in the regioselective
741 metabolism of toluene and o-, m- and p-xylene. *J. Pharmacol. Exp. Ther.* **1996,** *276* (1), 101-108.

742 (77) Zhao, B.; Guengerich, F. P.; Bellamine, A.; Lamb, D. C.; Izumikawa, M.; Lei, L.; Podust,
743 L. M.; Sundaramoorthy, M.; Kalaitzis, J. A.; Reddy, L. M.; Kelly, S. L.; Moore, B. S.; Stec, D.;
744 Voehler, M.; Falck, J. R.; Shimada, T.; Waterman, M. R. Binding of two flaviolin substrate
745 molecules, oxidative coupling, and crystal structure of streptomyces coelicolor a3(2) cytochrome
746 p450 158a2. *J. Biol. Chem.* **2005,** *280* (12), 11599-11607.

747 (78) Zhao, B.; Lamb, D. C.; Lei, L.; Kelly, S. L.; Yuan, H.; Hachey, D. L.; Waterman, M. R.
748 Different binding modes of two flaviolin substrate molecules in cytochrome p450 158a1
749 (cyp158a1) compared to cyp158a2. *Biochemistry* **2007,** *46* (30), 8725-8733.

750 (79) Sangha, A. K.; Parks, J. M.; Standaert, R. F.; Ziebell, A.; Davis, M.; Smith, J. C. Radical
751 coupling reactions in lignin synthesis: A density functional theory study. *J. Phys. Chem. B* **2012,**
752 *116* (16), 4760-4768.

753 (80) Ritchie, T. J.; Macdonald, S. J. The impact of aromatic ring count on compound
754 developability--are too many aromatic rings a liability in drug design? *Drug Discov. Today* **2009,**
755 *14* (21-22), 1011-1020.

756 (81) Peng, B.; Liu, M.; Han, Y.; Wanjaya, E. R.; Fang, M. L. Competitive biotransformation
757 among phenolic xenobiotic mixtures: Underestimated risks for toxicity assessment. *Environ. Sci.*
758 *Technol.* **2019,** *53* (20), 12081-12090.

(82) Totsuka, Y.; Hada, N.; Matsumoto, K.; Kawahara, N.; Murakami, Y.; Yokoyama, Y.; Sugimura, T.; Wakabayashi, K. Structural determination of a mutagenic aminophenylnorharman produced by the co-mutagen norharman with aniline. *Carcinogenesis* **1998,** *19* (11), 1995-2000.

SYNOPSIS GRAPHICS

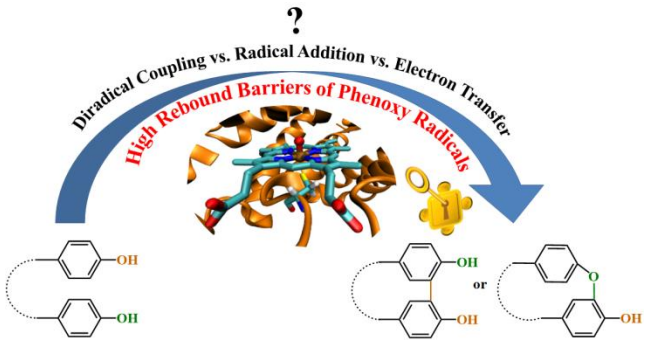

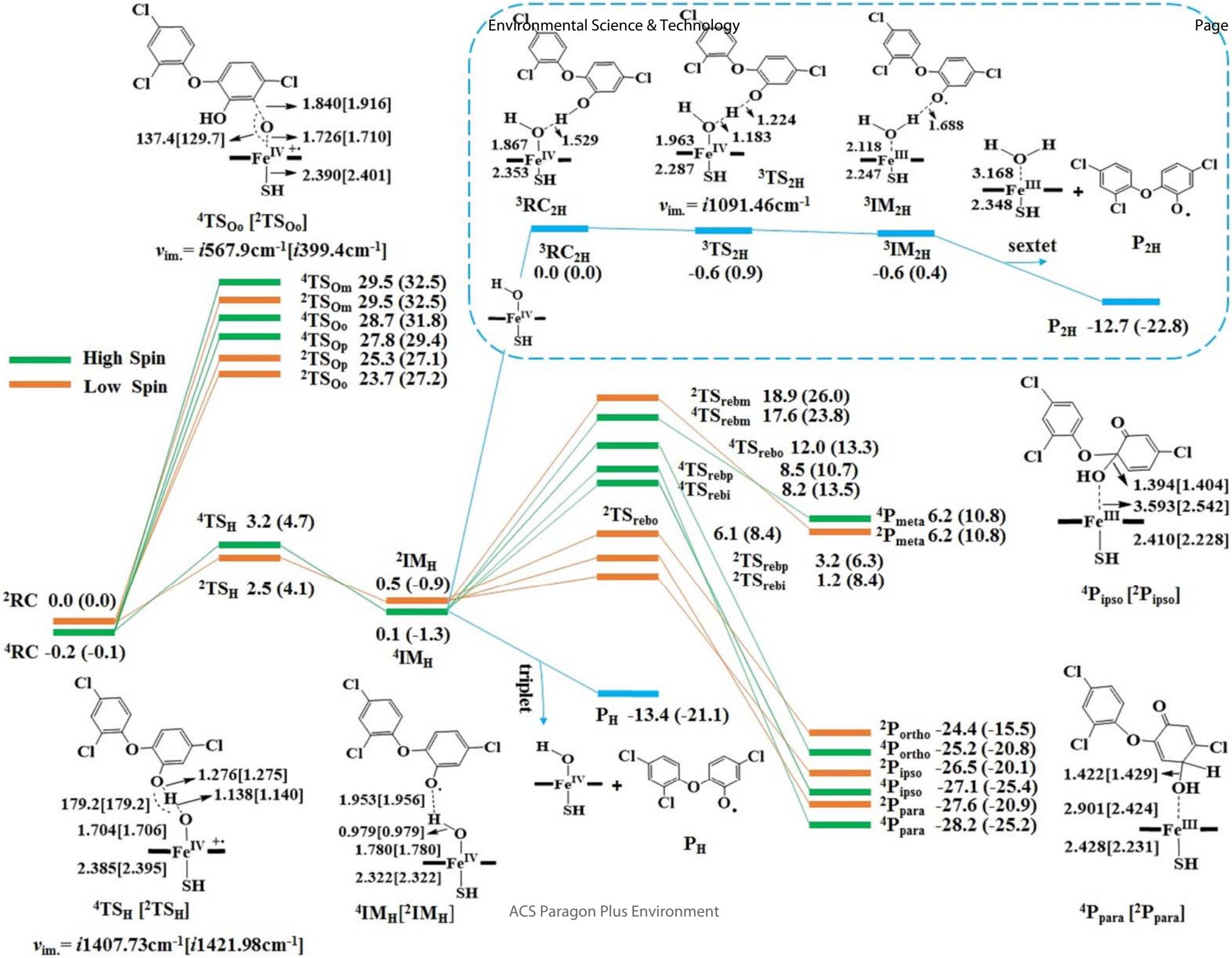
High Spin
Low Spin
$^4TS_{Oo}$ [$^2TS_{Oo}$]
$\nu_{im.}$ = i567.9cm^{-1}[i399.4cm^{-1}]
$^4TS_{Om}$ 29.5 (32.5)
$^2TS_{Om}$ 29.5 (32.5)
$^4TS_{Oo}$ 28.7 (31.8)
$^4TS_{Op}$ 27.8 (29.4)
$^2TS_{Op}$ 25.3 (27.1)
$^2TS_{Oo}$ 23.7 (27.2)
$^3RC_{2H}$
$\nu_{im.}$ = i1091.46cm^{-1}
$^3TS_{2H}$
$^3IM_{2H}$
$^3RC_{2H}$ 0.0 (0.0)
$^3TS_{2H}$ -0.6 (0.9)
$^3IM_{2H}$ -0.6 (0.4)
sextet
P_{2H}
P_{2H} -12.7 (-22.8)
$^2TS_{rebm}$ 18.9 (26.0)
$^4TS_{rebm}$ 17.6 (23.8)
$^4TS_{rebo}$ 12.0 (13.3)
$^4TS_{rebp}$ 8.5 (10.7)
$^4TS_{rebi}$ 8.2 (13.5)
$^4P_{meta}$ 6.2 (10.8)
$^2P_{meta}$ 6.2 (10.8)
$^2TS_{rebo}$ 6.1 (8.4)
$^2TS_{rebp}$ 3.2 (6.3)
$^2TS_{rebi}$ 1.2 (8.4)
$^4P_{ipso}$ [$^2P_{ipso}$]
^4TS_H 3.2 (4.7)
^2TS_H 2.5 (4.1)
^2IM_H 0.5 (-0.9)
^2RC 0.0 (0.0)
^4RC -0.2 (-0.1)
0.1 (-1.3) ^4IM_H
triplet
P_H -13.4 (-21.1)
$^2P_{ortho}$ -24.4 (-15.5)
$^4P_{ortho}$ -25.2 (-20.8)
$^2P_{ipso}$ -26.5 (-20.1)
$^4P_{ipso}$ -27.1 (-25.4)
$^2P_{para}$ -27.6 (-20.9)
$^4P_{para}$ -28.2 (-25.2)
P_H
^4TS_H [^2TS_H]
$\nu_{im.}$ = i1407.73cm^{-1}[i1421.98cm^{-1}]
^4IM_H[^2IM_H]
$^4P_{para}$ [$^2P_{para}$]